Development of a Two-Dimensional Zonally Averaged Statistical–Dynamical Model. Part I: The Parameterization of Moist Convection and its Role in the General Circulation

MAO-SUNG YAO

M/A-COM Sigma Data, Inc., NASA/Goddard Space Flight Center, Institute for Space Studies, New York, NY 10025

PETER H. STONE*

NASA/Goddard Space Flight Center, Institute for Space Studies, New York, NY 10025

(Manuscript received 20 March 1986, in final form 21 July 1986)

ABSTRACT

The moist convection parameterization used in the GISS 3-D GCM is adapted for use in a two-dimensional (2-D) zonally averaged statistical–dynamical model. Experiments with different versions of the parameterization show that its impact on the general circulation in the 2-D model does not parallel its impact in the 3-D model unless the effect of zonal variations is parameterized in the moist convection calculations. A parameterization of the variations in moist static energy is introduced in which the temperature variations are calculated from baroclinic stability theory, and the relative humidity is assumed to be constant. Inclusion of the zonal variations of moist static energy in the 2-D moist convection parameterization allows just a fraction of a latitude circle to be unstable and enhances the amount of deep convection. This leads to a 2-D simulation of the general circulation very similar to that in the 3-D model.

The experiments show that the general circulation is sensitive to the parameterized amount of deep convection in the subsident branch of the Hadley cell. The more there is, the weaker are the Hadley cell circulations and the westerly jets. The experiments also confirm the effects of momentum mixing associated with moist convection found by earlier investigators and, in addition, show that the momentum mixing weakens the Ferrel cell. An experiment in which the moist convection was removed while the hydrological cycle was retained and the eddy forcing was held fixed shows that moist convection by itself stabilizes the tropics, reduces the Hadley circulation, and reduces the maximum speeds in the westerly jets.

1. Introduction

In recent years a very large variety of climate models has been developed, ranging from latitudinally varying heat balance models and globally averaged radiative–convective models to three-dimensional general circulation models (GCMs). The value of such a variety of models has been emphasized by Schneider and Dickinson (1974) who advocated the development and use of a whole hierarchy of models, ranging from the simple one-dimensional (1-D) models to the complicated three-dimensional (3-D) models, as an aid in gaining understanding of the physical processes involved and of their interactions. Indeed, in our experience most of the progress that has been made in identifying the important climate processes has come from experiments with the simplified models and comparisons of these experiments with 3-D experiments (e.g., Hansen et al., 1984). In practice less effort has been devoted to two-dimensional (2-D) models than to 1-D and 3-D models. For example, the National Academy of Science's assessments of the sensitivity of climate to changes in carbon dioxide concentrations relied exclusively on results from 1-D and 3-D models (NAS, 1979, 1982 and 1983).

However our climate-modeling capability is still too rudimentary not to take advantage of a major class of models with unique capabilities, such as the zonal-mean 2-D models. These models can include interactions which are in principle excluded from 1-D models, e.g., the interaction between latitudinal and vertical structure and between latitudinal and vertical fluxes. These interactions are potentially very important in determining climate sensitivity (Stone and Carlson, 1979; Stone, 1984; Wang et al., 1984). At the same time a 2-D model is computationally more efficient than a 3-D model, typically being about two orders of magnitude faster. This greater efficiency can be crucial, for example, in problems involving very long time integrations, or problems requiring the inclusion of complex interactive chemical models. Equally important, this efficiency allows one to use 2-D models to make more comprehensive parametric studies of important climate processes than would be possible

* Also affiliated with Center for Meteorology and Physical Oceanography, Massachusetts Institute of Technology, Cambridge, MA 02139.

with a 3-D model. For example, 2-D models have been used to study the dependence of the general circulation on heat and momentum sources (Schneider, 1977, 1984) and the dependence of the Hadley cell on surface friction (Held and Hou, 1980).

An accurate simulation of the 2-D interactions in a 2-D model does require adequate parameterizations of large-scale eddy fluxes, and the lack of such parameterizations may well have been a factor in limiting the effort devoted to these models. However, new parameterizations of the eddy heat fluxes which for the first time include realistic β-effects and give good results when compared with observations have recently become available (Branscome, 1980, 1983). Consequently, the performance of the 2-D zonal-mean models needs to be reexamined.

This paper is intended to be the first in a series describing the development and application of a 2-D zonal-mean statistical–dynamical model. Earlier work on this kind of model is reviewed by Saltzman (1978) and Taylor (1980). Our model will differ from the earlier models in its parameterization of the eddy fluxes and variances, which will be based on Branscome's (1983) work. Other important differences from many of the earlier models will be the inclusion of a comprehensive hydrological cycle and radiation treatment and high vertical resolution (typically nine levels).

In addition, an important strategic difference between our work and earlier work is the manner in which our model has been and is being developed—namely, it is being developed explicitly as one of a hierarchy of climate models at the Goddard Institute for Space Studies (GISS). Others in this hierarchy are a 1-D globally averaged radiative–convective model (Lacis et al., 1981) and a 3-D GCM (Hansen et al., 1983). Developing the model as one in a hierarchy has two major advantages. First, identical parameterizations can be used in the different models, for example, the same radiation scheme is used in all three GISS models. This greatly facilitates intercomparison of model results and the diagnosis of the role of physical processes included in one model but not in another. Second, it is possible to use other model results as controls for the model under investigation. For example, all 2-D models which parameterize eddy effects have used eddy parameterizations based on theories for transient eddies arising from baroclinic instability. Validating these parameterizations by comparing model results with observations is problematic because the observations include the effects of stationary eddies forced by topography and ocean–continent contrasts. These effects are a priori excluded from 2-D zonal-mean models. However, with a 3-D GCM available one can run the 3-D model with all forcing for stationary eddies removed, and use the results as a proper control for validating the 2-D model's transient eddy parameterizations. This approach helps minimize differences between the models which arise from their different structures rather than from different physics, and again facilitates intercomparison and diagnosis of model results.

Another very important dynamical process that needs to be parameterized in both 2-D and 3-D models is moist convection. Experiments with 3-D models have shown that the general circulation is strongly dependent on the moist convection parameterization (Baker et al., 1977). The need to parameterize both moist convection and large-scale eddies introduces an essential complication in the development of a 2-D model, because the large-scale eddies and moist convection interact. Thus, a parameterization of moist convection which works well in a 1-D model where large-scale eddies are ignored or in a 3-D model where large-scale eddies are calculated explicitly, will not in general work well in a 2-D model with parameterized large-scale eddies. The problem is particularly acute in a 2-D model which has high vertical resolution like ours. Most other 2-D zonally averaged statistical–dynamical models have either omitted the hydrological cycle or used such low vertical resolution that no explicit moist convection was included. The only such model that has explicitly incorporated any effects of moist convection is the Lawrence Livermore Laboratory model (MacCracken, 1973). In that model the transports due to moist convection are parameterized in terms of the zonal mean relative humidity and vertical gradient of equivalent potential temperature.

In this first paper on our 2-D model we will focus on the development of the parameterization of moist convection. The problem of parameterizing the large-scale eddies will be dealt with in subsequent papers. To develop the moist convection parameterization, we performed 2-D experiments in which the eddy statistics were specified from a control run with a 3-D model which is a semispectral version of the GISS Model II GCM (Hansen et al., 1983). Thus, in section 2 we describe our 2-D model while in section 3 we describe the 3-D semispectral model and the control run itself. In section 4 we describe the impact of various parameterizations of moist convection on the general circulation of the 2-D model and report on experiments leading to the choice of a final parameterization. In this section we also describe an experiment illustrating the impact of moist convection on the general circulation. Finally in section 5 we summarize our results and discuss their implications.

2. Description of the 2-dimensional zonally averaged model

a. Basic equations and numerics

In our model we use the primitive equations in sigma and spherical coordinates. Using an overbar to represent a zonal average and a prime for deviation from the zonal average, and assuming that the surface pressure has no eddies, we can write the equations in the following flux forms. The continuity equation:

$$\frac{\partial}{\partial t}\left(\frac{\bar{\pi}}{mn}\right)+\frac{\partial}{\partial \eta}\left(\frac{\bar{\pi}\bar{v}}{m}\right)+\frac{\partial}{\partial \sigma}\left(\frac{\bar{\pi}\dot{\bar{\sigma}}}{mn}\right)=0, \tag{1}$$

the equations of motion:

$$\frac{\partial}{\partial t}\left(\frac{\bar{\pi}}{mn}\bar{u}\right)+\frac{\partial}{\partial \eta}\left(\frac{\bar{\pi}\bar{v}}{m}\bar{u}\right)+\frac{\partial}{\partial \sigma}\left(\frac{\bar{\pi}\dot{\bar{\sigma}}}{mn}\bar{u}\right)-\left[\frac{f}{mn}-\bar{u}\frac{\partial}{\partial \eta}\left(\frac{1}{m}\right)\right]\bar{\pi}\bar{v}$$
$$=\frac{\bar{\pi}}{mn}\bar{F}_\xi-\frac{\partial}{\partial \eta}\left(\frac{\bar{\pi}}{m}\overline{u'v'}\right)-\frac{\partial}{\partial \sigma}\left(\frac{\bar{\pi}}{mn}\overline{u'\dot{\sigma}'}\right)-\bar{\pi}\overline{u'v'}\frac{\partial}{\partial \eta}\left(\frac{1}{m}\right), \tag{2}$$

$$\frac{\partial}{\partial t}\left(\frac{\bar{\pi}}{mn}\bar{v}\right)+\frac{\partial}{\partial \eta}\left(\frac{\bar{\pi}\bar{v}}{m}\bar{v}\right)+\frac{\partial}{\partial \sigma}\left(\frac{\bar{\pi}\dot{\bar{\sigma}}}{mn}\bar{v}\right)$$
$$+\left[\frac{f}{mn}-\bar{u}\frac{\partial}{\partial \eta}\left(\frac{1}{m}\right)\right]\bar{\pi}\bar{u}+\frac{\bar{\pi}}{m}\left[\frac{\partial \bar{\Phi}}{\partial \eta}+\sigma\bar{\alpha}\frac{\partial \bar{\pi}}{\partial \eta}\right]$$
$$=\frac{\bar{\pi}}{mn}\bar{F}_\eta-\frac{\partial}{\partial \eta}\left(\frac{\bar{\pi}}{m}\overline{v'^2}\right)-\frac{\partial}{\partial \sigma}\left(\frac{\bar{\pi}}{mn}\overline{v'\dot{\sigma}'}\right)+\bar{\pi}\overline{u'^2}\frac{\partial}{\partial \eta}\left(\frac{1}{m}\right), \tag{3}$$

the first law of thermodynamics:

$$\frac{\partial}{\partial t}\left(\frac{\bar{\pi}}{mn}C_p\bar{T}\right)+\frac{\partial}{\partial \eta}\left(\frac{\bar{\pi}\bar{v}}{m}C_p\bar{T}\right)+\bar{p}^K\frac{\partial}{\partial \sigma}\left(\frac{\bar{\pi}\dot{\bar{\sigma}}}{mn}C_p\bar{\theta}\right)$$
$$-\bar{\pi}\sigma\bar{\alpha}\left[\frac{\partial}{\partial t}\left(\frac{\bar{\pi}}{mn}\right)+\frac{\bar{v}}{m}\frac{\partial \bar{\pi}}{\partial \eta}\right]$$
$$=\frac{\bar{\pi}}{m}\bar{Q}-\frac{\partial}{\partial \eta}\left(\frac{\bar{\pi}}{m}C_p\overline{v'T'}\right)-\bar{p}^K\frac{\partial}{\partial \sigma}\left(\frac{\bar{\pi}}{mn}C_p\overline{\dot{\sigma}'\theta'}\right)$$
$$-\bar{\pi}\sigma\frac{\overline{\alpha'v'}}{m}\frac{\partial \bar{\pi}}{\partial \eta}, \tag{4}$$

or

$$\frac{\partial}{\partial t}\left(\frac{\bar{\pi}}{mn}\bar{\theta}\right)+\frac{\partial}{\partial \eta}\left(\frac{\bar{\pi}\bar{v}}{m}\bar{\theta}\right)+\frac{\partial}{\partial \sigma}\left(\frac{\bar{\pi}\dot{\bar{\sigma}}}{mn}\bar{\theta}\right)$$
$$=\frac{\bar{\pi}}{c_pmn}\left(\overline{\frac{\theta}{T}Q}\right)-\frac{\partial}{\partial \eta}\left(\frac{\bar{\pi}}{mn}\overline{v'\theta'}\right)-\frac{\partial}{\partial \sigma}\left(\frac{\bar{\pi}}{mn}\overline{\dot{\sigma}'\theta'}\right), \tag{5}$$

and the moisture conservation equation:

$$\frac{\partial}{\partial t}\left(\frac{\bar{\pi}}{mn}\bar{q}\right)+\frac{\partial}{\partial \eta}\left(\frac{\bar{\pi}\bar{v}}{m}\bar{q}\right)+\frac{\partial}{\partial \sigma}\left(\frac{\bar{\pi}\dot{\bar{\sigma}}}{mn}\bar{q}\right)$$
$$=\frac{\bar{\pi}}{mn}(-\bar{C}+\bar{E})-\frac{\partial}{\partial \eta}\left(\frac{\bar{\pi}}{m}\overline{v'q'}\right)-\frac{\partial}{\partial \sigma}\left(\frac{\bar{\pi}}{mn}\overline{\dot{\sigma}'q'}\right). \tag{6}$$

The symbols are defined in Table 1. The temperatures above the dynamically active portion of the atmosphere ($P < P_T$) are determined by radiative equilibrium; $P'_s = 0$ by assumption.

The prognostic equations (1)–(6) will be solved numerically as an initial value problem. These equations together with the equation of state, $P = \rho RT$, and the hydrostatic equation, $\partial\Phi/\partial\sigma = -\pi\alpha$, form a complete set of equations provided that sink and source terms and eddy transports and variances are parameterized.

TABLE 1. Symbols used.

P	pressure
P_S	surface pressure
P_T	fixed pressure at top of the atmosphere, 10 mb
σ	$(P - P_T)/(P_S - P_T)$
π	$P_S - P_T$
ξ	longitude
η	latitude
a	earth's radius
m	$(a\cos\eta)^{-1}$
n	a^{-1}
t	time
α	(density)$^{-1}$
u	zonal wind speed
v	meridional wind speed
T	temperature
q	specific humidity
f	Coriolis parameter
z	height
Φ	geopotential
k	R/C_P
R	gas constant
C_p	specific heat at constant pressure
θ	T/P^k
C	rate of condensation
E	rate of evaporation
F_ξ, F_η	frictional forces in the zonal and meridional directions
$\dot{\sigma}$	$d\sigma/dt$
Q	heating rate per unit mass

We use nine σ-layers in the vertical with $\sigma = 1$ at the ground and $\sigma = 0$ at $P = P_T$. It is required that

$$\dot{\sigma}=0 \quad \text{at} \quad \sigma=0, 1. \tag{7}$$

The same σ levels as in Hansen et al. (1983) are used here (see Table 2). For vertical differencing schemes we employ those developed by Arakawa (1972) in designing the UCLA general circulation model.

For the meridional differencing we use a relatively coarse grid size, as in Hansen et al. (1983). The grid size is about 8° latitude (7.826° to be precise). As shown in Fig. 1, we use a staggered grid distribution; we carry pressure, temperature and specific humidity at points indicated by a dot, and horizontal winds at points between the dots (as shown with arrows). This grid arrangement corresponds to the B-scheme of Arakawa. The prognostic equations in finite-difference form are given in appendix A. These forms have the following integral conservation properties: advection conserves mass, potential temperature, the second moment of potential temperature and horizontal momentum globally; the vertically integrated pressure gradient force conserves momentum except for the force of the surface on the atmosphere; advection conserves kinetic energy; the Coriolis force term conserves kinetic energy, and total energy is conserved globally. These conservation properties minimize the spurious sources and sinks introduced by the finite difference approximations.

Even though many integral properties are main-

TABLE 2. Mean pressures of the nine σ-levels.

Level	Sigma	Pressure (mb)
9	.017	27
8	.095	103
7	.196	201
6	.319	321
5	.470	468
4	.640	634
3	.797	786
2	.907	894
1	.974	959

tained, two dimensional models need some damping to eliminate two-grid-size noise (e.g., Hunt, 1973). Here, we apply an eighth-order Shapiro filter (Shapiro, 1970) on surface pressure and potential temperature every hour. No other horizontal or vertical diffusion is used.

For the time differencing scheme we adopt the system used by Hansen et al. (1983). The source terms are calculated explicitly once every hour. The non-source terms are integrated using a leapfrog scheme initiated each hour with an Euler-backward step. The time step is 15 minutes.

All of the numerical schemes described above parallel those in the GISS Model II GCM (Hansen et al., 1983).

b. The model physics

The model physics is basically the same as the Model II physics of the GISS GCM (Hansen et al., 1983). However, it turns out that the Model I moist convection of Hansen et al. is more appropriate for our model, because the eddies' effect on moist convection can be included. The parameterization for moist convection will be described in more detail in section 4. Here, we only briefly describe the model physics. For a more detailed description of the parameterizations the reader may refer to Hansen et al. (1983).

Surface grid points are divided into land, ocean, and sea-ice fractions, as in the 3-D model. We do not plan to parameterize the dynamical effect of topography. [Omitting the heat transports associated with stationary eddies will not lead to major differences from the current zonal mean climate because the transports by transient eddies, which will be included, provide a strong negative feedback on the temperature structure (Stone, 1984).] The land and sea-ice temperatures are calculated from heat balance. Eventually we will use simple models for the ocean temperature and sea-ice cover analogous to those used in the GISS 3-D model (Hansen et al., 1984). However, in all the calculations reported here, the land fractions are set equal to zero, and the ocean sea-surface temperature and fractional ice cover are specified from the zonally averaged monthly mean data of Robinson and Bauer (1981), Walsh and Johnson (1979) and Alexander and Mobley (1974). Antarctica is replaced by sea-ice. Snow may fall on the sea-ice and affect its properties. Interactions between the surface and the atmosphere (radiation, momentum transfer and latent and sensible heat fluxes) are computed separately for the different surface types. Surface momentum transfer and latent and sensible heat fluxes are calculated with the same drag laws as in the GISS Model II GCM.

The radiatively active constituents in the atmosphere are H_2O, CO_2, O_3, O_2, NO_2, N_2O and CH_4 gases, clouds and aerosols. In the model only the distribution of H_2O and clouds are calculated, the remaining constituents being specified. The radiative heating includes contributions by both solar radiation and terrestrial thermal radiation. The method for solving the radiative transfer equations is the correlated k-distribution method, which is a generalization of the k-distribution method used by Lacis and Hansen (1974). The radiative calculations include all significant atmospheric constituents and employ realistic spectral properties of clouds and aerosols, based on Mie scattering computations. For convenience, in many of our experiments the diurnal cycle is not included, but we have studied its effect (see section 4).

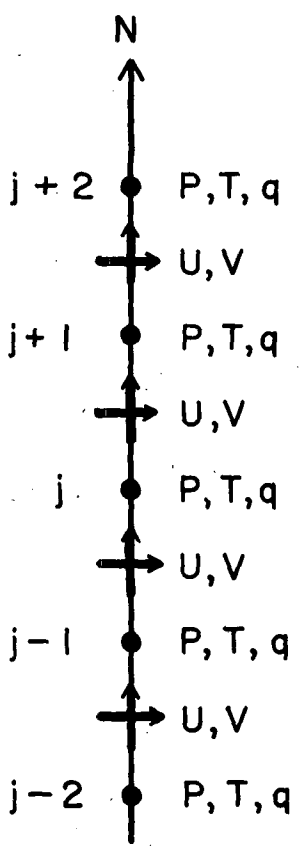

FIG. 1. Staggered grid used for meridional differencing in the 2-D model.

Large-scale condensation and associated clouds occur in an atmospheric layer for which the relative humidity exceeds 100%. In the experiments described here the cloud cover is prescribed based on the 3-D control simulation described in section 3. The final 2-D model will calculate clouds, but the necessary parameterizations may prove to be different from the 3-D model parameterizations.

3. The control run

a. The semispectral model

A modified version of the GISS Model II GCM, which generates eddies explicitly and uses surface conditions identical to those of the 2-D model, was used to produce a control experiment for the 2-D model. To make the 2-D and 3-D models compatible, we used the same meridional differencing schemes and a spectral expansion in the zonal direction. Using a spectral method one can avoid aliasing errors arising from quadratic nonlinearity and preserve the accuracy of evaluation of the zonal advection (cf. Bourke et al., 1977). In this semispectral model we used basically the same techniques of spectral analysis used by Held and Suarez (1978). Only wavenumbers $n \cdot K$ are allowed, where $n = 0, 1, 2, 3 \cdots n_m$, and n_m and K are integers which are specified in each experiment; $K_m = n_m K$ is the largest wavenumber retained. For example, if $n_m = 3$, then we have wavenumbers 0, 1, 2, 3 if $K = 1$, but 0, 3, 6, 9 if $K = 3$. In the control run described here, we use $n_m = 9$ and $K = 1$. The "transform method" (Orszag, 1970; Eliasen et al., 1970) is used for more efficient computation. For this procedure $3K_m + 1$ grid points along a latitude circle are used (cf. Bourke et al., 1977). (However, 36 grid points are used in physics calculations, as chosen by Hansen et al., 1983, in their medium grid model.) Detailed finite difference schemes and numerical techniques are not shown here and will be presented in a separate paper along with other experiments conducted with the semispectral model. Except for the semispectral representation the schemes parallel the GISS Model II GCM.

In order to eliminate computational problems near the poles, our integration domain is from 86.087°S to 86.087°N, and the first and last temperature (or pressure) points are at 82.174°S and 82.174°N, respectively. In addition, we have no eddies at the temperature points at 82.174°N/S, and $K_m = 3$ for horizontal winds at 78.261°N/S. The computational problem is due to the decreasing wave-scale toward the poles, and is particularly pronounced in semispectral models (e.g., Hunt, 1974; Held and Suarez, 1978). Except for a smoothing operator and the wave truncation near the poles, we do not need any other damping mechanisms such as a Shapiro filter (Hunt, 1974), or nonlinear horizontal diffusion (Hunt, 1974; Held and Suarez, 1978). For the time differencing scheme, for consistency we adopted the same system as the two-dimensional model and the GISS Model II GCM. More efficient semi-implicit schemes have not been implemented. (Our relatively coarse resolution is already rather efficient.)

The physics used in the semispectral model is the same as in the two-dimensional model except that here we have diurnal variations and the model II moist convection of Hansen et al. (1983) is used (see section 4). Thus, the semispectral model with appropriate boundary conditions is essentially the same as the GISS grid point Model II—only the zonal variations are handled differently. If $n_m = 9$ and $K = 1$, the zonal resolution of the semispectral model is roughly equivalent to that of the grid model with 10° longitudinal resolution.

b. The control run using the semispectral model

The numerical simulation with the semispectral model described here is intended to serve as a control for the development of our 2-D model. Thus the control run's boundary conditions are the same as for the experiments with the 2-D model described in subsequent sections, except that the 3-D model contains a diurnal cycle whereas the 2-D model does not. The effects of the diurnal cycle are, however, very small (see section 4b). The initial conditions for both models are actual data for 1 December 1976 (zonal mean data for the 2-D model). The calendar is fixed at 16 January for the specification of solar radiation parameters, sea surface temperature, and fraction of sea ice at the surface. Since continents and topography are omitted, eddies in the surface pressure field in the control run are negligible compared to eddies in the fields of meridional velocity, moisture, etc. Thus, the 2-D model assumption, $P'_s = 0$, has no significant impact on the comparisons with the control run. In order to ensure that an equilibrium state has been reached, the control integration is carried out for eight months and the last month is used for comparison with the 2-D model simulations.

Various fields from the control run's final month will be presented in the following sections where they will be compared directly with the 2-D model results. There is no point in making a detailed comparison between these fields and observations, because of the major differences between the boundary conditions for the simulation and for the real atmosphere. However, the semispectral model has also been used to simulate a realistic January, using the same zonal resolution as in the control run, but with realistic boundary conditions, identical to those used in the January simulations with the GISS 8° × 10° Model II GCM (Hansen et al., 1983). Table 3 compares a few key statistics of the general circulation taken from these two realistic 3-D simulations and from observations. Both the simulations started from actual data for 1 December 1976, and were carried out to the end of January 1977, to obtain January mean statistics. In the case of the GISS Model II GCM the integration was carried further, for a total

TABLE 3. January GCM simulations compared with observations.

	Northern Hemisphere				Southern Hemisphere			
	Jet stream		Hadley cell		Jet stream		Hadley cell	
Source	Strength ($m\ s^{-1}$)	Location (deg)	Strength ($10^9\ kg\ s^{-1}$)	Location (deg)	Strength ($m\ s^{-1}$)	Location (deg)	Strength ($10^9\ kg\ s^{-1}$)	Location (deg)
GISS Model II GCM	33	31	132	16	28	31	49	23
Semispectral Model	38	31	126	16	30	47	53	23
Observations (Oort, 1983)	40	30	194	10	24	40	27	20

of five years, and the five Januaries were averaged together to produce the January mean statistics presented in Hansen et al. (1983). However, for the statistics presented in Table 3 the differences between the initial January and the 5 Januaries' mean were negligible.

As one would expect from the close similarity of the 3-D models' numerics and physics, the January simulations are similar. The most notable difference is in the location of the Southern Hemisphere jet stream, which differs by two grid points in the two simulations. Compared with the observations the two simulations are about equally good. In fact, given the resolution of the 3-D models, the sparseness of data in the tropics and the Southern Hemisphere, and the sensitivity of the strength of the observed Hadley cells to the method of analysis, the agreement of both 3-D models with the observations is satisfactory (see also Hansen et al., 1983). We conclude that the semispectral model is a reasonable one to use for our control run.

We do document here the mean eddy fields produced by the final month of the control run, since they are used as specified forcings in all the 2-D model experiments reported in this paper. Figures 2–5 show the eddy kinetic energy and the meridional eddy transports of dry static energy, moisture, and zonal momentum, respectively. We note that the Northern Hemisphere fields are qualitatively similar to the total (transient plus stationary) eddy fields observed in the Northern Hemisphere winter. Figures 6–8 show the vertical eddy transports of dry static energy, moisture, and zonal momentum. The eddy temperature variance is necessary for one of the moist convection parameterizations described in the next section, but it is always parameterized and never specified from the control run.

4. Moist convection

a. Moist convection parameterizations

The moist convection parameterization developed for the GISS 3-D GCM was already available for use in our 2-D model. This parameterization is of the penetrating convection type. It provides for the mixing of sensible heat, moisture, and horizontal momentum between layers which are conditionally unstable. Supersaturation leads to condensation and precipitation, and the precipitation is allowed to reevaporate as it falls through lower layers. In order to keep the 2-D model physics as similar as possible to the 3-D model physics, we decided to adapt the 3-D model parameterization for use in the 2-D model. Hansen et al. (1983) give details of the scheme.

In fact, two different versions of the scheme were developed and evaluated by Hansen et al. The primary difference between the two versions was whether or not the lower layer's temperature was assumed to be uniform within a grid box. In the Model I version, the temperature in the lower layer was assumed to have a Gaussian distribution about the mean, with the variance of the distribution being determined by extrapolating the longitudinal temperature variance at model resolved scales down to the subgrid scale. In the Model II version the lower layer temperature was assumed to be uniform within the grid box. Thus in Model I there

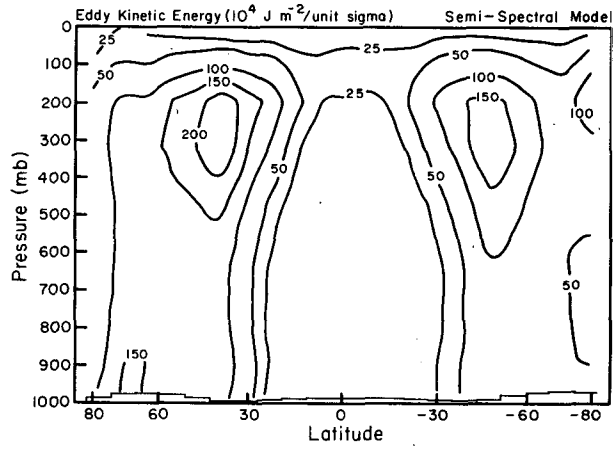

FIG. 2. Pressure–latitude cross section of the zonal mean eddy kinetic energy from the 3-D control run. Units are 10^4 J m^{-2} (unit sigma)$^{-1}$.

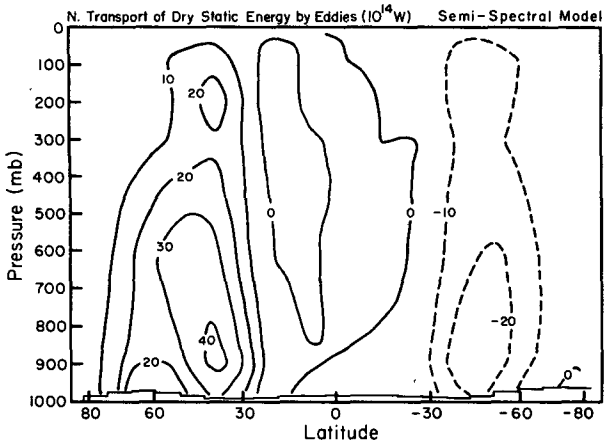

FIG. 3. As in Fig. 2 but for northward transport of dry static energy by eddies. Units are 10^{14} W.

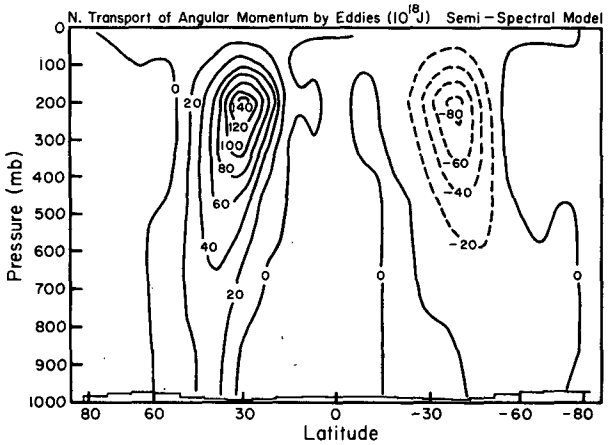

FIG. 5. As in Fig. 2 but for northward transport of angular momentum by eddies. Units are 10^{18} J.

was a distribution of moist static energies associated with the lower layer, and consequently it was possible for a fraction of the layer to be unstable with respect to higher layers, and only this fraction would participate in the mixing process. In contrast in Model II either all or none of the layer was unstable, and in the unstable case 50% of the layer always participated in the mixing process. The only other appreciable difference between the two versions was that, in Model I, layers below the condensation level were not allowed to participate in the moist convection process, while in Model II they were.

The differences between the large-scale fields of temperature, moisture, and winds produced by the 3-D GCM using the two different parameterizations were relatively minor and did not noticeably favor either scheme. Consequently the computationally more efficient version, i.e., the Model II version, was selected as the standard version for use with the 3-D model. However, the Model I version is in principle more realistic, since it allows for convection to develop on smaller and more realistic scales than the resolution of the 3-D model (8° of latitude by 10° of longitude). Also, one would expect the differences between simulations with the two versions to be magnified as the model's resolution is made cruder. A 2-D model such as ours represents an extreme in this sense, since in this model the Model II parameterization would require 50% of the whole latitude circle to convect if any convection at all is to occur at that latitude. Thus one might well anticipate that the Model I approach would be significantly better for the 2-D model even if it isn't for the 3-D model. In fact one difference between the two approaches that was apparent to a small degree in the 3-D experiments proved to be a crucial difference in the 2-D model. That is, the Model I scheme yields

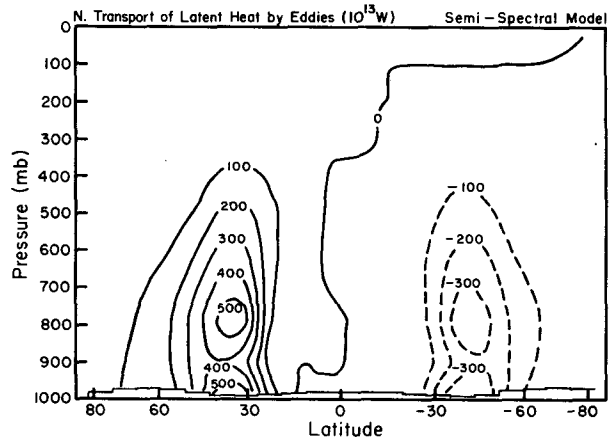

FIG. 4. As in Fig. 2 but for northward transport of latent heat by eddies. Units are 10^{13} W.

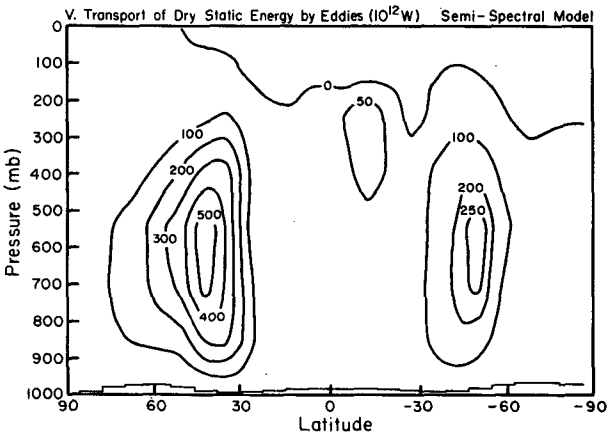

FIG. 6. As in Fig. 2 but for vertical transport of dry static energy by eddies. Units are 10^{12} W.

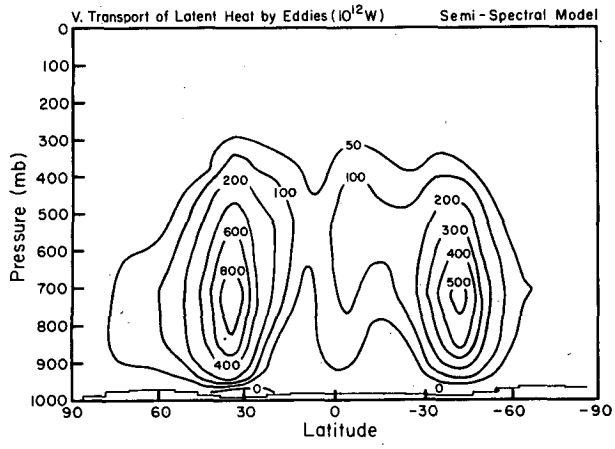

FIG. 7. As in Fig. 2 but for vertical transport of latent heat. Units are 10^{12} W.

more deep convection than the Model II scheme because of the subgrid scale temperature variance (Hansen et al., 1983).

However the Model I version cannot be directly implemented in the 2-D model, because the 2-D model has no longitudinal resolution at all from which one can extrapolate to obtain a subgrid-scale variance. Thus we had to derive a separate parameterization for this temperature variance. To do this we assumed that the temperature variations around a latitude circle occur primarily in middle and high latitudes, and that these variations are due to eddies arising from baroclinic instability. This variance can be estimated by using the method of Branscome (1983). The vertical structure is calculated from an approximate solution for the most unstable mode in Charney's (1947) model of baroclinic instability, and the amplitude is calculated by equating the eddy kinetic energy of the most unstable mode to the mean available potential energy defined for a meridional scale equal to the radius of deformation. Branscome (1983) gives parameterizations calculated in this way for the eddy heat fluxes. The result for the zonal mean temperature variance is (Branscome, personal communication, 1980)

$$\overline{T'^2} = (N^2)_w \left[\frac{T_w H_w}{g(1+\gamma)}\left(\frac{\partial u}{\partial z}\right)_w\right]^2 \left(1 - \frac{z(1+\gamma)}{2H_w}\right) e^{-z(1+\gamma)/H_w} \tag{8}$$

where T is the temperature, N the Brunt–Väisälä frequency, H the scale height, g the acceleration of gravity, z the height above the surface, u the zonal wind, and γ is

$$\gamma = \frac{H_w (N^2)_w \beta}{f^2 (\partial u/\partial z)_w}. \tag{9}$$

Also f is the Coriolis parameter and β is the derivative of f with respect to meridional position. The subscript w in all cases refers to vertically averaged values of the respective quantities, weighted by the depth of the most unstable eddy, e.g.,

$$(N^2)_w = \frac{\int_0^\infty N^2 e^{-z(1+\gamma)/H} dz}{\int_0^\infty e^{-z(1+\gamma)/H} dz}. \tag{10}$$

Time and zonal mean temperature variances associated with observed transient eddies have been calculated, for example, by Oort and Peixoto (1983). However, these observed variances include two contributions, one due to propagating eddies and one due to standing eddies which fluctuate on time scales less than a month. Our parameterization is meant to represent just the first of these two contributions to the observed variance. Thus, we cannot make a direct comparison between our parameterization and the observations. We do note that if we apply Eq. (8) to calculate T'^2 from observations of the zonal mean fields, it does have magnitudes and vertical variations which resemble those of the observed T'^2 in the subtropics and midlatitudes, but its magnitude is much smaller than the observed magnitude in high latitudes. Also we note that in the 3-D control run the eddy variance peaked in midlatitudes and at zonal wavenumber 6. Therefore, a parameterization based on the most unstable baroclinic wave appears to be appropriate. In the real world another source of zonal variance is land–ocean contrasts. Since our model does allow grid points to have land fractions, this variance could also be included. For convenience it is omitted in the experiments reported here, where we use an all ocean lower boundary.

Near the equator, $f \to 0$, $\gamma \to \infty$, and the baroclinic eddy variance $\to 0$, i.e., baroclinic instability will give rise to very little temperature variance in the tropics.

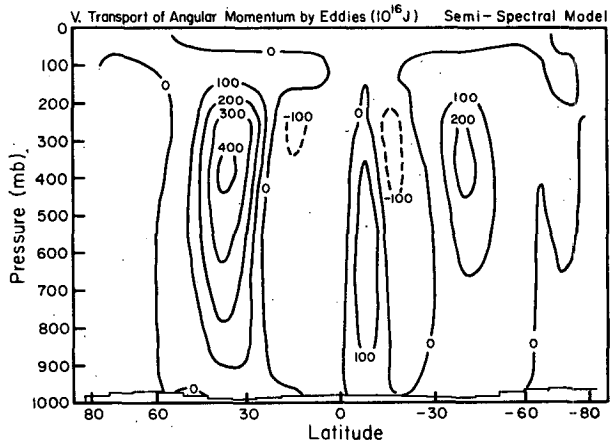

FIG. 8. As in Fig. 2 but for vertical transport of angular momentum by eddies. Units are 10^{16} J.

However, one would expect some variance to be present even at the equator because of other sources—e.g., tropical waves—and observations do show transient eddy variances on synoptic time scales of order $2K^2$ near the equator (Oort and Peixoto, 1983). Therefore we supplemented the above parameterization by adding to it a fixed variance of $2K^2$ at all locations. The effect of this additional variance turned out to be very small (see below).

b. *Experiments with the parameterizations*

With the above parameterization for $\overline{T'^2}$ it is possible to use either the Model I parameterization or the Model II parameterization (which requires no modification) in our 2-D model. To simplify the analysis of the impact of these parameterizations on the large-scale fields, in all our 2-D model experiments the eddy terms in the prognostic equations were assigned monthly mean values taken from the control run of the 3-D semispectral model described in section 3b. Thus we could eliminate imperfections in the parameterizations of the eddy fluxes and wind variances as a source of differences between the zonal mean fields produced by the experiments and the control run. For the same reason cloud cover was also assigned values taken from the control run. However, the radiative fluxes, large scale condensation, and surface fluxes were calculated in the experiments. Although the radiative fluxes are strongly constrained by the specification of the clouds and sea surface temperatures, they can still respond to changes in the atmospheric temperature and moisture fields. Thus, the surface fluxes, large scale condensation, and, to a certain extent, the radiative fluxes interact with the moist convective fluxes in the experiments.

In all the 2-D experiments described below no diurnal cycle was included—i.e., the sun had a fixed zenith angle, varying with latitude, picked to give the proper amount of incident short wave radiation on 16 January. Separate experiments showed that including a diurnal cycle generally had a negligible effect on the results reported here—e.g., changes in the mean zonal winds were only a few tenths of a meter per second. This is not surprising in view of the fact that the 2-D model had an all ocean lower boundary, except for sea ice near the poles. Indeed the only significant effect of the diurnal cycle that we found was on the albedos of the sea ice near the South Pole. Variations in sea ice can be important in some climate experiments and it would be appropriate to include the diurnal cycle in such experiments with the 2-D model. Similarly it should be included when fractional land grid points are included. Aside from the lack of diurnal variations, the zonal mean initial conditions and boundary conditions in all of the experiments described below were identical to those used in the control run. All experiments were integrated for 8 months, and the results shown are for the mean state during the final month of the integrations. All of the differences we discuss, based on the final months of the 2-D and 3-D integrations, are much larger than the month to month changes in the last months of the integrations.

To evaluate the different parameterizations, the 2-D model was integrated twice, once with the Model I parameterization of moist convection, and once with the Model II parameterization. We will refer to these experiments as 2DMI and 2DMII, respectively. Figures 9–11 illustrate the moist convective heating rates produced by the control run of the semispectral model, the 2DMI experiment, and the 2DMII experiment, respectively.

The 2-D experiments with both parameterizations differ substantially from the control run in the lowest layer of the tropical atmosphere, where they have positive heating rates rather than negative heating rates. This is caused by the higher relative humidities in this layer in the symmetric model, about 90%, compared to about 80% in the 3-D model. The higher humidity reduces the reevaporation of precipitation falling through this layer and thus warms the layer. However, this difference is largely compensated by increased longwave cooling and does not have much impact on the rest of the 2-D model simulation (see section 4c). We note that positive heating rates in the lowest layer in the tropics are realistic (Johnson, 1984), and also occur in the 3-D grid model when the resolution is increased. In the 3-D model experiment with greater resolution (described by Hansen et al., 1983) the positive heating rates are also associated with higher relative humidities in the lowest layer.

The higher relative humidities in the lowest layer of the tropics in the 2-D model and in the 3-D model with increased resolution are in part due to a smaller amount of moist convection in the subtropics. This reduces the flux of moisture from the lower troposphere to the upper troposphere, which allows higher humidities to build up in the subtropical atmosphere. The

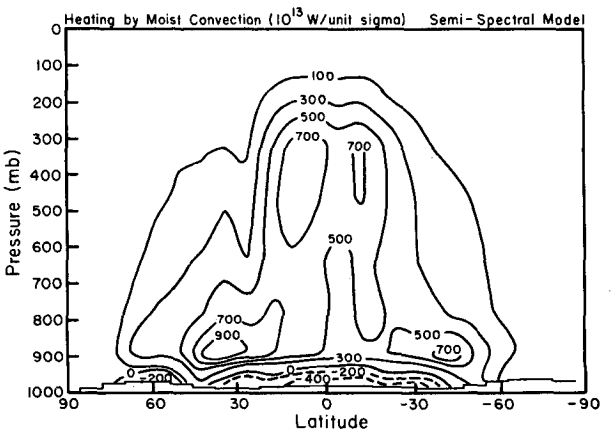

FIG. 9. Pressure–latitude cross section of heating by moist convection from the 3-D control run. Units are 10^{13} W (unit sigma)$^{-1}$.

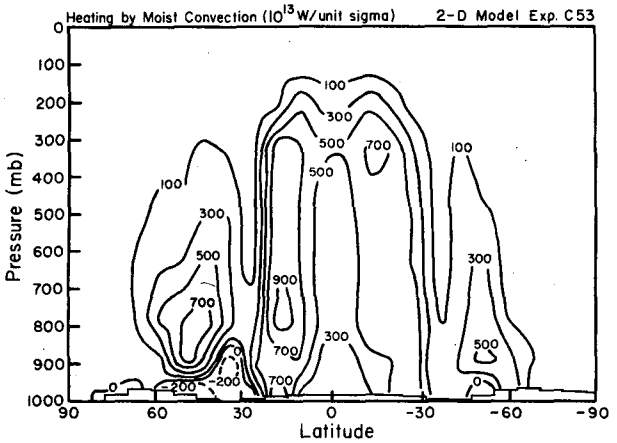

FIG. 10. As in Fig. 9 but from the 2-D simulation with Model I moist convection.

equatorward branch of the Hadley cell then transports more water vapor into the tropics than it would do otherwise. The higher humidities are also in part due to the equatorward branch being more highly concentrated near the ground (see section 4c).

Otherwise, Figs. 9–11 show that both of the 2-D parameterizations produce heating rates that are similar in magnitude and sign to those in the control run. However, there are important differences in the distribution of the heating. Both parameterizations give a double intertropical convergence zone (ITCZ) which is too strong compared to the 3-D simulation. The deficiency is more severe in the 2DMII experiment than in the 2DMI experiment. In addition both parameterizations give too strong a minimum in the subtropics, i.e., in the region of subsidence; again the deficiency is more severe in 2DMII than in 2DMI. Finally, the height to which the convective heating extends in midlatitudes in the control run is simulated reasonably well in 2DMI, but not as well in 2DMII.

A less direct but very important test of the parameterizations is their impact on the general circulation. Figure 12 illustrates the mean zonal wind fields produced at 201 mb by the 3-D control run and the 2DMI and 2DMII experiments. Here we see a large quantitative difference produced by the two different parameterizations. In general, the Model II parameterization leads to midlatitude zonal winds much stronger than in the control run, while the Model I parameterization leads to midlatitude zonal winds which are only slightly too strong. For example, the Northern Hemisphere westerly jet maximum in 2DMI is about 20% stronger than in the control run, but in 2DMII it is 70% stronger. Also the easterly winds in the tropics are much too strong in 2DMII.

The differences in the zonal winds are caused by the different amounts of deep convection in the subtropics. Increases in the deep convection weaken the subtropical subsidence and decrease the strength of the Hadley cells. (The Hadley cell from several experiments is illustrated in sections 4c and 5.) This decrease is accompanied by a decrease in the Hadley cells' poleward angular momentum transport and this leads to a decrease in the strength of the midlatitude jet streams. In our experiments the zonal winds are quite sensitive to the amount of deep convection in the subtropics.

The preceding results led us to select the Model I parameterization of moist convection for use in the 2-D model. We performed additional experiments to determine the sensitivity of the 2-D model's simulation to some of the arbitrary features of the parameterization of the temperature variance. In one experiment the minimum variance was eliminated and in another it was doubled to $4K^2$. The impact was small; the changes in the convective heating rates were negligible in midlatitudes and were typically about 3% near the equator, and the jet stream maxima changed by 5% or less.

Another arbitrary feature built into the Model I moist convection parameterization is the assumption that the specific humidity is uniform within a grid box, so that the variance in moist static energy is due solely to the parameterized variance in the temperature. To test this assumption we performed an experiment in which the relative humidity instead of the specific humidity was assumed to be a constant. This will increase the variance of moist static energy around a latitude circle and do it in a way that is physically plausible. That is, the large ocean surface at the lower boundary should tend to produce uniform relative humidities instead of uniform specific humidities, both in our model and in the real world.

Figure 13 shows the heating by moist convection from the 2-D simulation when the constant relative humidity assumption is made. Comparing this figure with Fig. 10, we see that the increased variance in the moist static energy gives rise to more deep convective heating, particularly in the subtropics. Compared to the amount of deep convective heating in the control

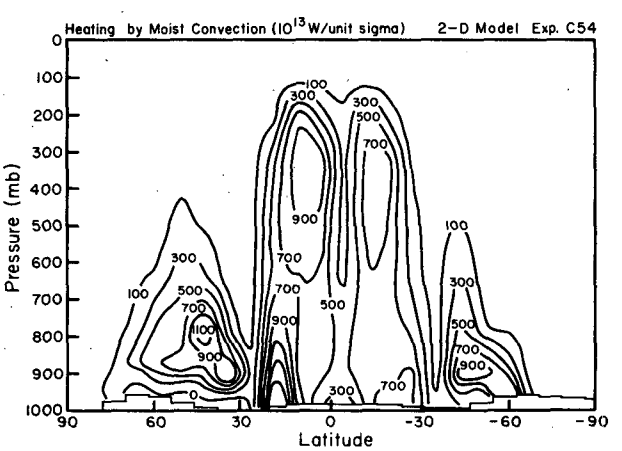

FIG. 11. As in Fig. 9 but from the 2-D simulation with Model II moist convection.

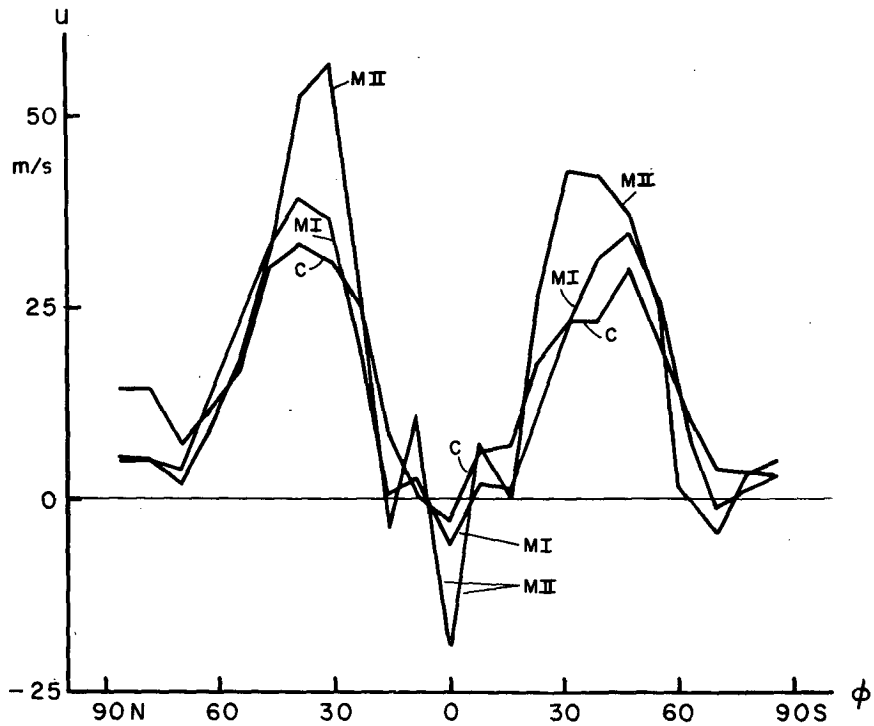

FIG. 12. Zonal mean zonal wind vs latitude at 201 mb produced by the 3-D control run (C), the 2-D simulation with model I moist convection (MI), and the 2-D simulation with model II moist convection (MII).

run (see Fig. 9) this is an improvement. The comparisons with the control run's precipitation and evaporation were also improved in the subtropics. The greater amount of deep convection increased the flux of moisture from the lower troposphere to the upper troposphere, thereby causing an increase in both the surface

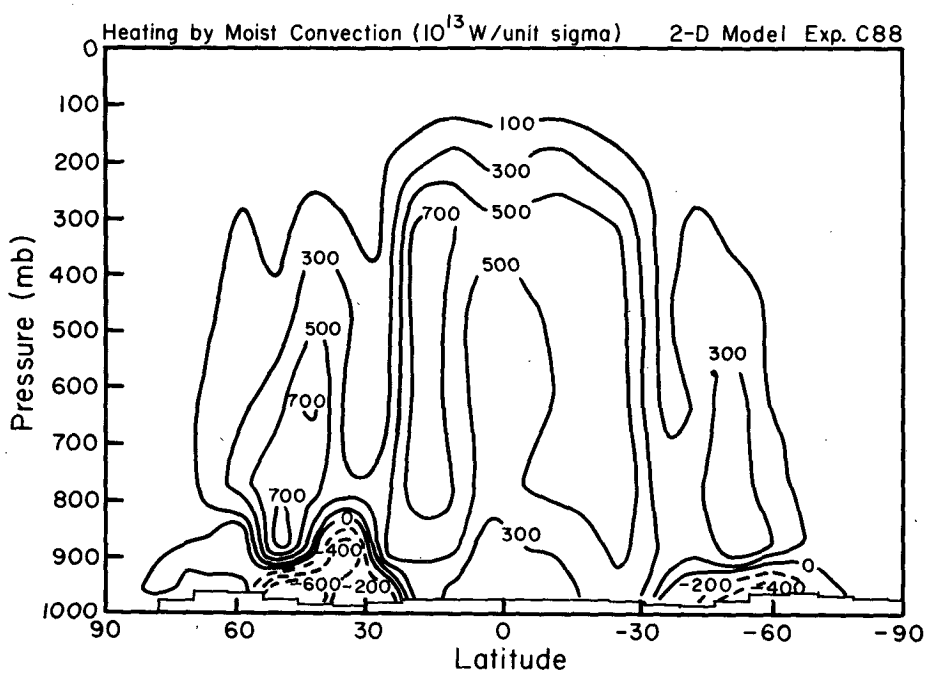

FIG. 13. As in Fig. 9 but from the 2-D simulation with Model I moist convection calculated with a constant relative humidity assumption instead of constant specific humidity.

evaporation and the convective precipitation. In contrast the comparisons of the same fields in midlatitudes with the control run were degraded by the assumption of constant relative humidity. However, these changes were generally considerably smaller than the beneficial changes in the subtropics.

Figures 14 and 15 show the zonal wind fields from the control run and from the 2-D experiment with the assumption of constant relative humidity in the moist convection parameterization. The agreement between them is excellent, and in fact better than when constant specific humidity is assumed. For example, in the 2-D simulation with the constant relative humidity assumption the maximum westerly winds in the Northern and Southern hemisphere jet streams and the maximum low-level easterly wind in the tropics exceed those in the control run by only 1.2, 1.1 and 3.9 m s^{-1}, respectively, while in the simulation with constant specific humidity the excesses were 5.8, 4.8 and 4.6 m s^{-1}, respectively. The improvement in the jet streams again results from the increased moist convective heating in the subtropics, which reduces the subsidence in the subtropics, the circulation in the Hadley cell, the poleward transport of angular momentum by the Hadley cell, and the speed of the jet streams. These results led us to adopt the assumption of constant relative humidity for the final form of our moist convection parameterization.

Since the effect of moist convection on the momentum balance of the atmosphere is not well known, an important question is: to what extent is the impact of our parameterization on the zonal winds due to our inclusion of mixing of horizontal momentum? To determine this we performed an additional experiment, using the final form for our parameterization of moist convection, but with the mixing of horizontal momentum eliminated. The effect of eliminating the momentum mixing is illustrated in Fig. 16, which shows the mean zonal wind from this last experiment. This

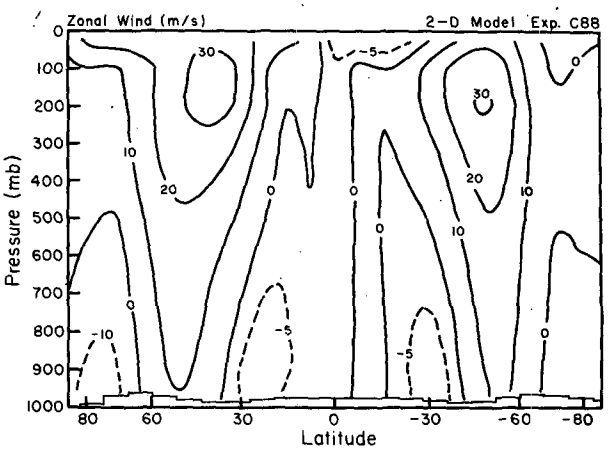

FIG. 15. As in Fig. 14 but from the 2-D simulation with Model I moist convection using a constant relative humidity.

field may be compared with the result when the mixing was included, shown in Fig. 15. The momentum mixing has a large effect in the tropics and the Southern Hemisphere subtropics, where it reduces the wind shear substantially. This same effect was present in the 3-D grid model (Hansen et al., 1983). However, the momentum mixing does not contribute much to the impact of moist convection on the midlatitude jet streams. In the 3-D model the simulation was improved by the momentum mixing, and so it was retained (Hansen et al., 1983). In order to make the 2-D model parallel the 3-D model as much as possible, we have also retained the momentum mixing in our 2-D model.

c. *Additional tests of the final parameterization*

The mean meridional circulations are also a valuable diagnostic of whether the moist convection parameterization is working well. Figures 17 and 18 show the streamfunction for the mean meridional circulation,

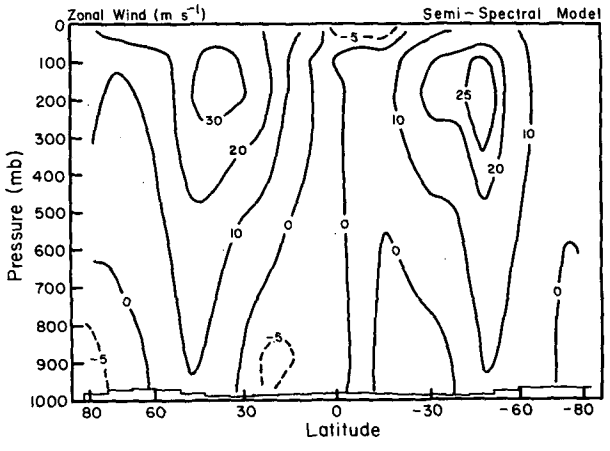

FIG. 14. Pressure–latitude cross section of the zonal mean zonal wind from the 3-D control run. Units are m s^{-1}.

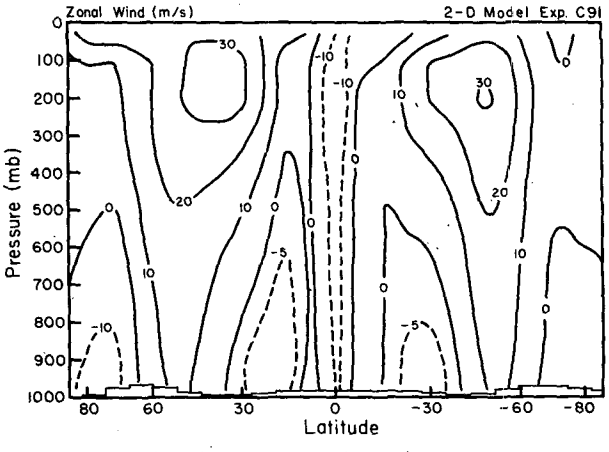

FIG. 16. As in Fig. 15 but with no momentum mixing by moist convection.

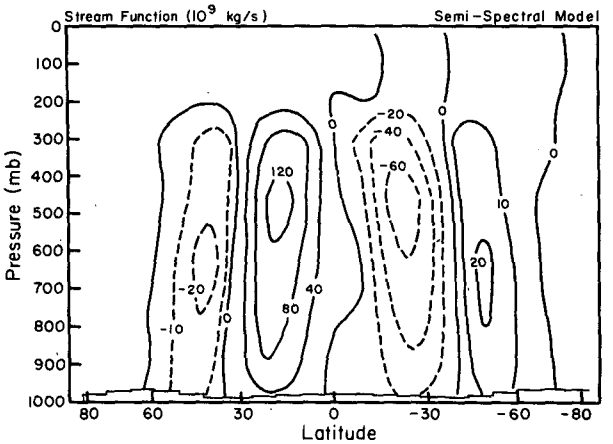

FIG. 17. Pressure–latitude cross section of the zonal mean stream function from the 3-D control run. Units are 10^9 Kg s^{-1}.

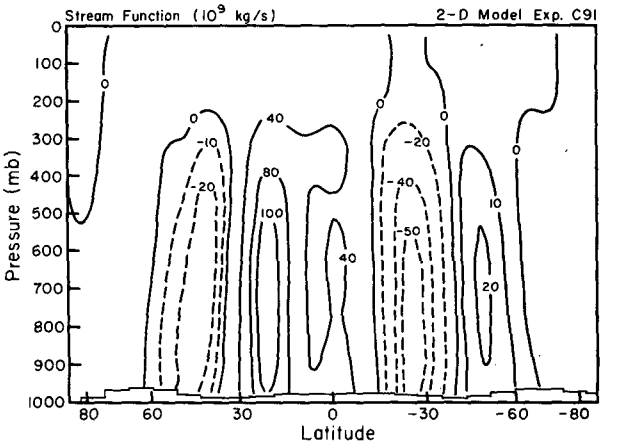

FIG. 19. As in Fig. 18 but with no momentum mixing by moist convection.

from the 3-D control run and from the 2-D model with the final moist convection parameterization, respectively. The 2-D model with the final moist convection parameterization simulates the control run's results for the meridional and vertical extents and the strength of the Hadley and Ferrel cells reasonably well. The most notable difference is that the meridional winds are more strongly concentrated near the surface in the 2-D model. This difference is one reason for the higher relative humidities near the surface in the tropics: since the specific humidity is strongly peaked at the surface, concentrating the equatorward branch of the Hadley cells near the surface increases the transport of moisture into lower latitudes.

Figure 19 shows the streamfunction simulated by the 2-D model when momentum mixing is omitted from the moist convection. Comparison of this figure with Fig. 18 shows that the impact of momentum mixing in the tropics is small. For example, in the experiment in which the momentum mixing associated with the moist convection was removed, the mass flux in the Northern Hemisphere Hadley cell was reduced only by about 15%, and the mass flux in the Southern Hemisphere Hadley cell was almost unchanged. The momentum mixing had a similar effect in the 3-D grid-point GCM (Model I), where its omission reduced the mass flux in the Northern Hemisphere Hadley cell by about 20% (Rind and Rossow, 1984). By contrast the momentum mixing has a significant impact on the Ferrel cells. This impact is due to the slight acceleration in the jet streams when the momentum mixing is removed. The resulting increase in equatorial Coriolis force aloft accelerates the circulation in the Ferrel cells. Although the changes in the zonal winds are small, the changes in the Ferrel cells are relatively large because they represent the net effect of forcings which individually produce direct or indirect cells. For example, the mass flux in the Northern Hemisphere Ferrel cell is increased by more than 50% if the momentum mixing is removed.

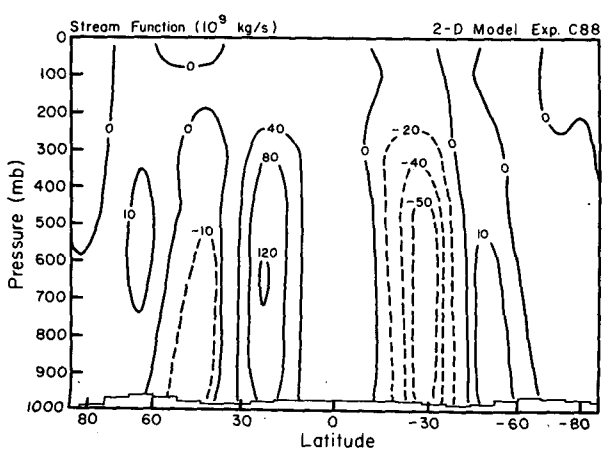

FIG. 18. As in Fig. 17 but from the 2-D simulation with the final moist convection parameterization.

Because of the strong interaction of the moist convection with the surface fluxes of heat, another valuable test of the moist convection parameterization is the simulation of the surface heat fluxes. In particular, the simulation of these fluxes will help evaluate one difference between the moist convection in the 2-D model and that in the 3-D model, i.e., the different sign of the heating rates in the lowest layer in the tropics. Figure 20 compares the surface evaporation and sensible heat fluxes from the control run and from the 2-D model simulation with the final moist convection parameterization. In fact, we see that these fluxes are reproduced quite well by the 2-D model in spite of the different sign of the moist convective heating rates in the lowest layer. This agreement is due to the strong negative feedback between moist convective heating and long-

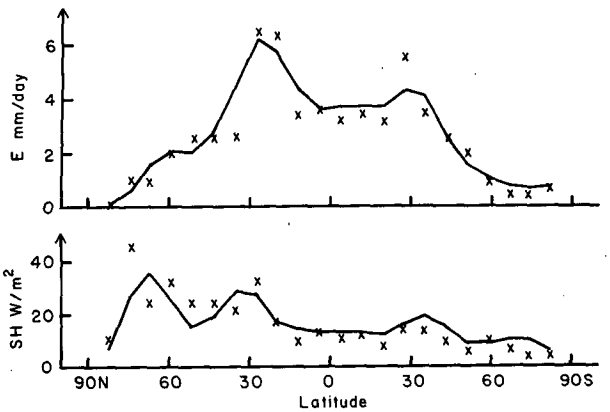

FIG. 20. (a) Zonal mean evaporation vs latitude from the 3-D control run (solid curve) and the 2-D simulation with the final moist convection parameterization (×'s). (b) As in (a) but for surface sensible heat flux.

wave cooling, i.e., the total heating rate due to both these processes in the lowest model layer in the tropics is about the same in both the control run and the 2-D simulation.

Finally, Fig. 21 illustrates the 2-D model's simulation of precipitation with the final moist convection parameterization. This also agrees well with the precipitation in the control run. The most notable difference is the stronger variations in precipitation rates in the subtropics and tropics in the 2-D model compared to the 3-D model. The stronger variations are of course related to the stronger variations in the convective heating rates in the 2-D model, i.e., stronger (weaker) heating rates are associated with more (less) convective precipitation. However to first order the global precipitation rates are the same: 3.4 mm day^{-1} in the control run and 3.1 mm day^{-1} in the 2-D model.

d. The role of moist convection

We performed an additional experiment with the 2-D model in which the parameterized moist convection was completely omitted. The difference between the simulated fields in this experiment and the 3-D control run provide a quantitative measure for judging the success of our moist convection parameterization. In addition, the experiment is of intrinsic interest for the insight it can yield about the role of moist convection in the general circulation. In the experiment dry convection was still allowed, and indeed it was much more active than when moist convection was included. However, the dry convection was active primarily in the two lowest model layers. In addition condensation due to supersaturation could still occur, and was quite important (see below). The dry convection and supersaturation condensation prevented the lapse rates from becoming statically unstable when the moist convection was eliminated.

Figures 22 and 23 show the zonal mean zonal wind and streamfunction fields from the experiment with no moist convection. These may be compared with Figs. 14 and 17 which show the same two fields, respectively, from the control run. We see that moist convection does indeed have a very large impact. The meridional and zonal winds are much stronger in both low and middle latitudes in the absence of moist convection. The stronger circulations can be traced to the effect of moist convection on the tropical static stability. When the moist convection was removed, the static stability decreased and this enhanced the rising motion near the equator. This increased the moisture convergence and led to large amounts of large-scale saturation and condensation, so much that the condensation near the equator was *greater* than in the case when moist convection was present. (This is illustrated by the precipitation rates shown in Fig. 21.) The enhanced condensation increased the differential heating in latitude, further accelerating the whole Hadley circulation, and also limited the decrease in the tropical static stability. The acceleration of the Hadley circulation led to an

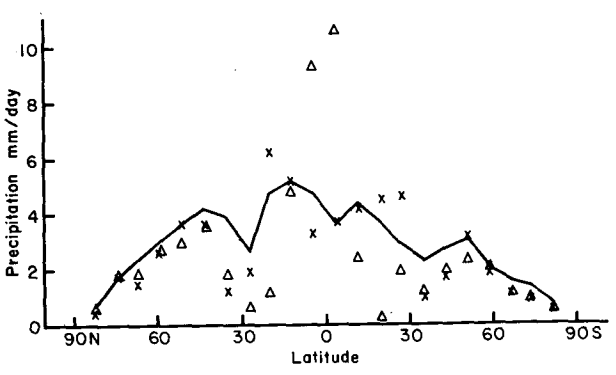

FIG. 21. Zonal mean precipitation vs latitude from the 3-D control run (solid curve), the 2-D simulation with the final moist convection parameterization (×'s), and the 2-D simulation with no moist convection (Δ's).

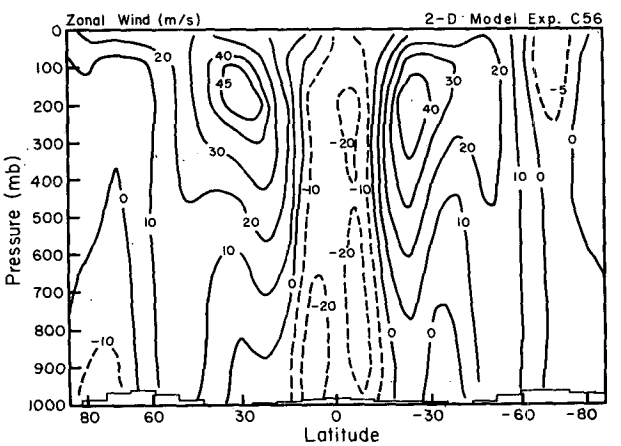

FIG. 22. As in Fig. 14 but from the 2-D simulation with no moist convection.

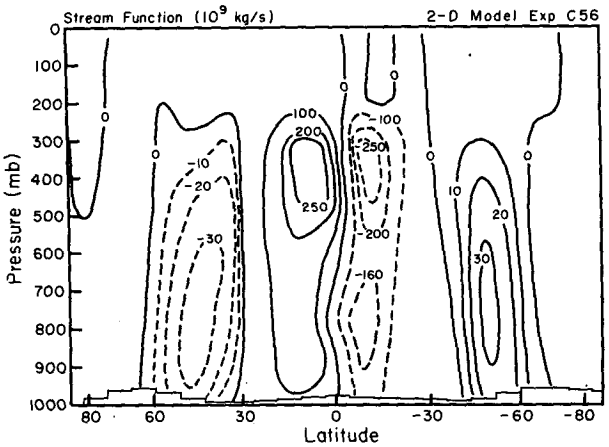

FIG. 23. As in Fig. 17 but from the 2-D simulation with no moist convection.

increase in the poleward transport of zonal angular momentum and an acceleration of the midlatitude jet streams. In the simulated Northern Hemisphere the net effect of removing the moist convection was a decrease of the mean static stability of the tropical troposphere from 3.9 to 3.1K km^{-1}, an increase in the Hadley cell mass flux by 140%, and an increase in the speed of the jet stream by 50%. These quantitative changes may depend on the particular parameterization of moist convection we have used, but the qualitative changes should not, since all moist convection parameterizations act to enhance the static stability.

Another feature of the experiment without moist convection was the disappearance of the double ITCZ. The low-latitude rising motions had a double maximum in the 3-D control run and in all the 2-D experiments except the one in which moist convection was omitted, e.g., compare Figs. 18 and 23. Why the double ITCZ should depend on the presence of moist convection is not apparent. We note that in our experiments the double ITCZ is not caused by a double maximum in the sea-surface temperature (SST). The specified SST has a single maximum at 4°N in all the experiments. The maximum rising motion in the experiment with no moist convection occurred at the equator, while the maxima in the control run and in the 2-D model with the final moist convection parameterization occurred near 12°N and 12°S. We also note that the double ITCZ occurs in the 3-D model even when realistic boundary conditions are used. For example, it is apparent in the January simulations with the GISS grid point model reported by Hansen et al. (1983). In those simulations it is not so clear cut in the zonal mean state as in our experiments because the double ITCZ is confined to the ocean areas in the Hansen et al. experiments. The 3-D grid GCM experiments also show that the two ITCZ's become sharper and move nearer the equator if the 8° × 10° resolution is improved to 4° × 5°.

Finally, we assess the success of the final moist convection parameterization by comparing the zonal mean zonal wind and stream function fields it produces (Figs. 15 and 18) with those produced by the control run (Figs. 14 and 17) and those produced without any moist convection (Figs. 22 and 23). We see that including the parameterization does indeed lead to a simulation of the general circulation in the 2-D model much closer to that in the 3-D control run.

5. Discussion

Our primary purpose has been to develop a parameterization of moist convection for use in a 2-D zonally averaged statistical–dynamical model. Our approach has been to generalize the parameterization used in a state-of-the-art 3-D climate model so that the impact on the general circulation in the 2-D model will parallel that in the 3-D model. To do this we found it necessary to parameterize the zonal variations of moist static energy. This was accomplished by calculating a temperature variance from baroclinic stability theory and calculating the specific humidity variance by assuming a constant relative humidity. The parameterized variations increased the amount of deep moist convection and led to a general circulation in the 2-D model which closely resembled that in the 3-D model. Differences remain between the 2-D and 3-D simulations, in particular the different sign of the moist convective heating rates in the lowest layer of the tropics, and the deeper moist convection and greater precipitation in the subtropics in the 3-D model. However, the 3-D grid-point simulations of these features with realistic boundary conditions are themselves not very realistic, and in any case the differences do not have much impact on the simulation of the general circulation.

Our results also agree with the results found by Baker et al. (1977) in experiments with a 3-D GCM, i.e., the simulation of the general circulation is sensitive to the parameterization of moist convection. They showed that changing from a convective adjustment scheme to a scheme similar to Kuo's (1965) led to major changes in the GCM's energy cycle and zonal mean vertical motions. The parameterizations we have investigated are all of the penetrating convection type, and our experiments used a 2-D model. Nevertheless, we also found that the energy levels and vertical motions were sensitive to how the convection was parameterized (results not shown). In addition our experiments indicate that the zonal mean zonal wind field is sensitive to the moist convection parameterization. In particular, in our experiments changes in the amount of deep convection in the region of Hadley cell subsidence were responsible for the sensitivity. Increases in the amount of deep convection in this region lead to decreases in the strength of the Hadley cell and its associated angular momentum transport, and thus to decreases in the strength of the jet streams. However, the

degree of sensitivity found in our experiments may not be realistic because the eddy statistics were not allowed to interact with the general circulation.

Our experiments also confirm the results of other 2-D and 3-D investigations of the impact of momentum mixing by moist convection. The momentum mixing substantially reduces the vertical shear of the zonal-mean zonal wind in the tropics, and increases the mass circulation in the Hadley Cell (Schneider and Lindzen, 1977; Schneider, 1977; Helfand, 1979; Hansen et al., 1983; Rind and Rossow, 1984). In addition our experiments showed another impact not looked for in the previous studies. That is, the Ferrel cell is also affected by the momentum mixing, with the cell's circulation being decreased by the addition of momentum mixing.

Finally, our experiments yield insight about the role of moist convection in the general circulation. To the best of our knowledge no other model, either 2-D or 3-D, has been used to examine the sensitivity of the general circulation to the addition or removal of just the process of moist convection. More typically, other experimenters have investigated the effect of adding the whole hydrological cycle. For example, Manabe et al. (1965) added a hydrological cycle to a 3-D GCM, and Schneider and Lindzen (1977) and Schneider (1977) simulated the addition of a hydrological cycle to a 2-D model. In these experiments the flux of heat into the atmosphere in low latitudes is increased by a substantial amount because of either the explicit or implicit addition of surface evaporation. The resulting condensation near the equator increases the meridional differential heating of the atmosphere substantially, accelerating the circulation in the Hadley cell and increasing the associated meridional transports.

In all our experiments, even without moist convection, the hydrological cycle was retained. The effects of *adding* moist convection are of course just the opposite of the effects of *removing* moist convection, which were the effects we discussed in section 4d. According to our results, if moist convection is added to a system which already has a hydrological cycle, the static stability increases, the convergence of moisture and precipitation near the equator decrease and the circulation in the Hadley cell and its associated transports decrease. Thus, the effect of adding moist convection by itself is just the opposite of the effect of adding the whole hydrological cycle.

In addition we found that the 2-D simulations contained a double ITCZ only when moist convection was present. We plan a separate series of experiments to investigate the cause of this phenomenon. Since the double ITCZ occurs in both 2-D and 3-D models, but is better defined in the 2-D model, this appears to be an example of a problem for which the 2-D model is ideally suited.

Acknowledgments. We are indebted to Gary Russell, Reto Ruedy, and Jean Lerner for their help with the diagnostic and physics routines from the GISS 3-D model; to Lee Branscome for supplying us with the eddy temperature variance from baroclinic stability theory; and to Tony DelGenio, David Rind, Bill Rossow, and an anonymous referee for reading the manuscript critically. This work was supported principally by the NASA Climate Program.

APPENDIX A

Prognostic Equations in Finite-Difference Form

Let the subscript j and superscript k be meridional (see Fig. 1) and vertical (see Fig. A1) grid indices, respectively, and define

$$\Pi_j \equiv \pi_j \left(\frac{\Delta\xi \Delta\eta}{mn}\right)_j, \quad \dot{S}_j^k \equiv \Pi_j \bar{\sigma}_j^k,$$

$$G_{j+1/2}{}^k \equiv \frac{1}{2}(\pi_j + \pi_{j+1}) \left(\bar{v}\frac{\Delta\xi}{m}\right)_{j+1/2}^k \tag{A1}$$

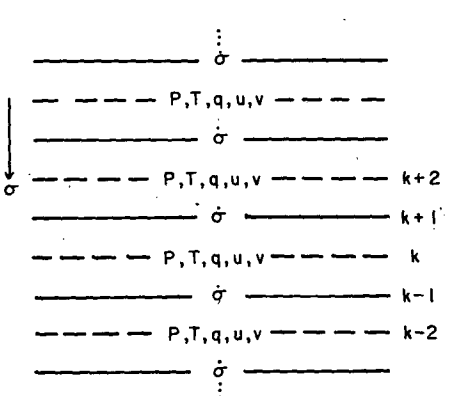

FIG. A1. Staggered grid used for vertical differencing in the 2-D model.

We can write Eqs. (1)–(6) in the following finite-difference form without eddy forcing terms. The continuity equation:

$$\frac{\partial \Pi_j}{\partial t} + G^k_{j+1/2} - G^k_{j-1/2} + \frac{1}{\Delta\sigma_k}(\dot{S}_j^{k-1} - \dot{S}_j^{k+1}) = 0 \tag{A2}$$

u-velocity equation:

$$\frac{\partial}{\partial t}(\Pi^{(u)}_{j+1/2}\bar{u}^k_{j+1/2}) + \frac{1}{4}[(G^k_{j+1/2} + G^k_{j+3/2})(\bar{u}^k_{j+1/2} + \bar{u}^k_{j+3/2}) - (G^k_{j-1/2} + G^k_{j+1/2})(\bar{u}^k_{j-1/2} + \bar{u}^k_{j+1/2})]$$

$$+ \frac{1}{\Delta\sigma_k}\frac{1}{2}[\dot{S}^{(u)k-1}_{j+1/2}(\bar{u}^{k-2}_{j+1/2} + \bar{u}^k_{j+1/2}) - \dot{S}^{(u)k+1}_{j+1/2}(\bar{u}^k_{j+1/2} + \bar{u}^{k+2}_{j+1/2})] - \frac{1}{4}[(\pi_j + \pi_{j+1})(C_j^k + C^k_{j+1})]\bar{v}^k_{j+1/2}$$

$$= \Pi_{j+1/2}(u)\bar{F}^k_{\xi j+1/2} \tag{A3}$$

where

$$C_j^k = f_j\left(\frac{\Delta\xi\Delta\eta}{mn}\right)_j - \frac{1}{2}(\bar{u}^k_{j+1/2} + \bar{u}^k_{j-1/2})\left[\left(\frac{\Delta\xi}{m}\right)_{j+1/2} - \left(\frac{\Delta\xi}{m}\right)_{j-1/2}\right] \tag{A4}$$

v-velocity equation:

$$\frac{\partial}{\partial t}(\Pi^{(v)}_{j+1/2}\bar{v}^k_{j+1/2}) + \frac{1}{4}[(G^k_{j+1/2} + G^k_{j+3/2})(\bar{v}^k_{j+1/2} + \bar{v}^k_{j+3/2}) - (G^k_{j-1/2} + G^k_{j+1/2})(\bar{v}^k_{j-1/2} + \bar{v}^k_{j+1/2})]$$

$$+ \frac{1}{\Delta\sigma_k}\frac{1}{2}[\dot{S}^{(v)k-1}_{j+1/2}(\bar{v}^{k-2}_{j+1/2} + \bar{v}^k_{j+1/2}) - \dot{S}^{(v)k+1}_{j+1/2}(\bar{v}^k_{j+1/2} + \bar{v}^{k+2}_{j+1/2})] + \frac{1}{4}[(\pi_j + \pi_{j+1})(C_j^k + C^k_{j+1})]\bar{u}^k_{j+1/2}$$

$$+ \left(\frac{\Delta\xi}{m}\right)_{j+1/2}\frac{1}{2}\{(\pi_j + \pi_{j+1})(\Phi^k_{j+1} - \Phi_j^k) + [(\pi\sigma\bar{\alpha})^k_{j+1} + (\pi\sigma\bar{\alpha})_j^k](\pi_{j+1} - \pi_j)\} = \Pi_{j+1/2}{}^{(v)}\bar{F}^k_{\eta j+1/2} \tag{A5}$$

the thermodynamic equation:

$$\frac{\partial}{\partial t}(\Pi_j\bar{T}_j^k) + \frac{1}{2}[G^k_{j+1/2}(\bar{T}_j^k + \bar{T}^k_{j+1}) - G^k_{j-1/2}(\bar{T}^k_{j-1} + \bar{T}_j^k)] + \frac{1}{\Delta\sigma_k}[\dot{S}_j^{k-1}\bar{\theta}_j^{k-1}(P_j^k)^K - \dot{S}_j^{k+1}\bar{\theta}_j^{k+1}(P_j^k)^K]$$

$$-\frac{1}{c_p}(\pi\sigma\bar{\alpha})_j^k\frac{\partial\Pi_j}{\partial t} - \frac{1}{4}\frac{1}{c_p}\left\{\left(\bar{v}\frac{\Delta\xi}{m}\right)^k_{j+1/2}[(\pi\sigma\bar{\alpha})^k_{j+1} + (\pi\sigma\bar{\alpha})_j^k](\pi_{j+1} - \pi_j) + \left(\bar{v}\frac{\Delta\xi}{m}\right)^k_{j-1/2}[(\pi\sigma\bar{\alpha})_j^k + (\pi\sigma\bar{\alpha})^k_{j-1}](\pi_j - \pi_{j-1})\right\}$$

$$= \frac{1}{c_p}\Pi_j\bar{Q}_j^k \tag{A6}$$

or

$$\frac{\partial}{\partial t}(\Pi_j\bar{\theta}_j^k) + \frac{1}{2}[G^k_{j+1/2}(\bar{\theta}_j^k + \bar{\theta}^k_{j+1}) - G^k_{j-1/2}(\bar{\theta}^k_{j-1} + \bar{\theta}_j^k)] + \frac{1}{\Delta\sigma_k}\frac{1}{2}[\dot{S}_j^{k-1}(\bar{\theta}_j^{k-2} + \bar{\theta}_j^k) - \dot{S}_j^{k+1}(\bar{\theta}_j^k + \bar{\theta}_j^{k+2})] = \frac{\Pi_j}{c_p}\left(\overline{\frac{\theta}{T}Q}\right)_j^k \tag{A7}$$

the moisture conservation equation:

$$\frac{\partial}{\partial t}(\Pi_j\bar{q}_j^k) + \frac{1}{2}[G^k_{j+1/2}(\bar{q}_j^k + \bar{q}^k_{j+1}) - G^k_{j-1/2}(\bar{q}^k_{j-1} + \bar{q}_j^k)] + \frac{1}{\Delta\sigma_k}\frac{1}{2}[\dot{S}_j^{k-1}(\bar{q}_j^{k-2} + \bar{q}_j^k) - \dot{S}_j^{k+1}(\bar{q}_j^k + \bar{q}_j^{k+2})]$$

$$= \Pi_j(\overline{-C+E})_j^k. \tag{A8}$$

For energy conservation, we require

$$\Pi_{j+1/2}{}^{(u)} = \Pi_{j+1/2}{}^{(v)} = \frac{1}{2}(\Pi_j + \Pi_{j+1})$$

$$\dot{S}_{j+1/2}{}^{(u)} = \dot{S}_{j+1/2}{}^{(v)} = \frac{1}{2}(\dot{S}_j + \dot{S}_{j+1}), \tag{A9}$$

at the poles, $C = 0$ in Eqs. (A3) and (A5), at the North Pole ($j = p$)

$$\Pi_{p-1/2}{}^{(u)} = \Pi_{p-1/2}{}^{(v)} = \Pi_p + \frac{1}{2}\Pi_{p-1}$$

$$\dot{S}_{p-1/2}{}^{(u)} = \dot{S}_{p-1/2}{}^{(v)} = \dot{S}_p + \frac{1}{2}\dot{S}_{p-1}; \tag{A10}$$

similarly for the South Pole.

We note that Eqs. (A2), (A3), (A5), (A6) and (A8) formally maintain the energy conservation law. In programming, Eq. (A7) is used instead of (A6) to save computer time. Thus, the formal guarantee of energy conservation is lost. But actual numerical integration does practically maintain the energy conservation. It can be shown that Eqs. (A2), (A3), (A5), (A6) and (A8) correspond to the symmetric version of Arakawa's design of the UCLA general circulation model (Arakawa, 1972). In applying Eq. (A8), schemes similar to those in Hansen et al. (1983) are used to prevent the occurrence of negative specific humidity.

REFERENCES

Alexander, R. C., and R. L. Mobley, 1974: Monthly average sea-surface temperatures and ice-pack limits on a 1° global grid. Rep. 4-1310-ARPA, Rand Corp., Santa Monica, 30 pp.

Arakawa, A., 1972: Design of the UCLA atmospheric general circulation model. Tech. Rep. No. 7, Dept. of Meteorology, University of California at Los Angeles.

Baker, W. E., E. Kung and R. C. J. Somerville, 1977: Energetics diagnosis of the NCAR general circulation model. *Mon. Wea. Rev.*, **105**, 1384–1401.

Bourke, W., B. McAvaney, K. Puri and R. Thuring, 1977: Global modeling of atmospheric flow by the spectral method. *Methods in Computational Physics*, No. 17, *General Circulation Models of the Atmosphere*, J. Chang, Ed., Academic Press, 267–324.

Branscome, L. E., 1980: Scales and structures of baroclinic waves and their influence on climatic states. Ph.D. thesis, Massachusetts Institute of Technology, 201 pp.

——, 1983: A parameterization of transient eddy heat flux on a beta-plane. *J. Atmos. Sci.*, **40**, 2508–2521.

Charney, J. G., 1947: The dynamics of long waves in a baroclinic westerly current. *J. Meteor.*, **4**, 135–163.

Eliasen, E., B. Machenhauer and E. Rasmussen, 1970: On a numerical method for integration of the hydrodynamical equations with a spectral representation of the horizontal fields. Rep. No. 2, Institute for Theoretical Meteorology, Copenhagen University, Haraldsgade 6, DK 2200, Copenhagen, N Denmark, 37 pp.

Hansen, J., G. Russell, D. Rind, P. Stone, A. Lacis, S. Lebedeff, R. Ruedy and L. Travis, 1983: Efficient three dimensional global models for climate studies: models I and II. *Mon. Wea. Rev.*, **111**, 609–662.

Hansen, J., A. Lacis, D. Rind, G. Russell, P. Stone, I. Fung, R. Ruedy and J. Lerner, 1984: Climate sensitivity: analysis of feedback mechanisms. *Climate Processes and Climate Sensitivity*, Amer. Geophys. Union, Geophys. Monogr. No. 29, 130–163.

Held, I. M., and M. Suarez, 1978: A two-level primitive equation atmospheric model designed for climatic sensitivity experiments. *J. Atmos. Sci.*, **35**, 206–229.

——, and A. Y. Hou, 1980: Nonlinear axially symmetric circulations in a nearly inviscid atmosphere. *J. Atmos. Sci.*, **37**, 515–533.

Helfand, H. M., 1979: The effect of cumulus friction on the simulation of the January Hadley circulation by the GLAS model of the general circulation. *J. Atmos. Sci.*, **36**, 1827–1843.

Hunt, B. G., 1973: Zonally symmetric global general circulation models with and without the hydrologic cycle. *Tellus*, **25**, 337–354.

——, 1974: A global general circulation model of the atmosphere based on the semispectral method. *Mon. Wea. Rev.*, **102**, 3–16.

Johnson, R. H., 1984: Partitioning tropical heat and moisture budgets into cumulus and mesoscale components: implications for cumulus parameterization. *Mon. Wea. Rev.*, **112**, 1590–1601.

Kuo, H.-L., 1965: On formation and intensification of tropical cyclones through latent heat release by cumulus convection. *J. Atmos. Sci.*, **22**, 40–63.

Lacis, A. A., and J. E. Hansen, 1974: A parameterization for the absorption of solar radiation in the earth's atmosphere. *J. Atmos. Sci.*, **31**, 118–133.

——, ——, P. Lee, T. Mitchell and S. Lebedeff, 1981: Greenhouse effect of trace gases, 1970–1980. *Geophys. Res. Lett.*, **8**, 1035–1038.

MacCracken, M. C., 1973: Zonal atmospheric model ZAM2. *Proc. Conf. Climatic Assessment Program, 2nd, U.S. Dept. Transportation*, DOT-TSC-OST-73-4, 298–320.

Manabe, S., J. Smagorinsky and R. Strickler, 1965: Simulated climatology of a general circulation model with a hydrologic cycle. *Mon. Wea. Rev.*, **93**, 769–798.

NAS, 1979: Carbon dioxide and climate: a scientific assessment. National Academy of Sciences-National Research Council, Washington, DC, 22 pp.

——, 1982: Carbon dioxide and climate: a second assessment. National Academy of Sciences-National Research Council, Washington, DC, 72 pp.

——, 1983: Changing climate. National Academy of Sciences-National Research Council, Washington, DC, 496 pp.

Oort, A. H., 1983: Global Atmospheric Circulation Statistics, 1958–73. NOAA Prof. Pap. No. 14, U.S. Dept. of Commerce, Washington, DC, 180 pp.

——, and J. P. Peixoto, 1983: Global angular momentum and energy balance requirements from observations. *Advances in Geophysics*, Vol. 25, Academic Press, 355–490.

Orszag, S. A., 1970: Transform method for the calculation of vector-coupled sums: application to the spectral form of the vorticity equation. *J. Atmos. Sci.*, **27**, 890–895.

Rind, D., and W. B. Rossow, 1984: The effects of physical processes on the Hadley circulation. *J. Atmos. Sci.*, **41**, 479–507.

Robinson, M., and R. Bauer, 1981: *Oceanographic Monthly Summary*, **1**, No. 2, NOAA National Weather Service, W322, Washington, DC, 2–3.

Saltzman, B., 1978: A survey of statistical–dynamical models of the terrestrial climate. *Advances in Geophysics*, Vol. 20, Academic Press, 183–304.

Schneider, E. K., 1977: Axially symmetric steady-state models of the basic state for instability and climate studies. Part II. Nonlinear calculations. *J. Atmos. Sci.*, **34**, 280–296.

——, 1984: Response of the annual and zonal mean winds and temperatures to variations in the heat and momentum sources. *J. Atmos. Sci.*, **41**, 1093–1115.

——, and R. E. Dickinson, 1974: Climate modeling. *Rev. Geophys. Space Phys.*, **12**, 447–493.

——, and R. S. Lindzen, 1977: Axially symmetric steady state models of the basic state for instability and climate studies. Part I. Linearized calculations. *J. Atmos. Sci.*, **34**, 263–279.

Shapiro, R., 1970: Smoothing, filtering and boundary effects. *Rev. Geophys. Space Phys.*, **8**, 359–387.

Stone, P. H., 1984: Feedbacks between dynamical heat fluxes and temperature structure in the atmosphere. *Climate Processes and Climate Sensitivity*. Amer. Geophys. Union, Geophys. Monogr. No. 29, 6–17.

——, and J. H. Carlson, 1979: Atmospheric lapse rate regimes and their parameterization. *J. Atmos. Sci.*, **36**, 415–423.

Taylor, K. E., 1980: The roles of mean meridional motions and large scale eddies in zonally averaged circulations. *J. Atmos. Sci.*, **37**, 1–19.

Walsh, J., and C. Johnson, 1979: An analysis of Arctic sea ice fluctuations. *J. Phys. Oceanogr.*, **9**, 580–591.

Wang, W.-C., G. Molnar, T. Mitchell and P. Stone, 1984: Effects of dynamical heat fluxes on model climate sensitivity. *J. Geophys. Res.*, **89**, 4699–4711.